JTTEE5 5:343-351

Characterization and Processing of Spray-Dried Zirconia Powders for Plasma Spray Application

P. Pei, S.G. Malghan, S.J. Dapkunas, and P.H. Zajchowski

The correlation between the performance of plasma spray coatings and feedstock powder properties is not fully understood. To demonstrate this correlation, eight spray-dried zirconia powders containing a mass fraction of 20 % Y_2O_3 (yttria) were characterized with respect to their physical, bulk chemical, and surface chemical properties. The same powders were plasma spray deposited as coatings, and their relative performance was evaluated using a thermal rupture test developed by Pratt and Whitney. The specific powder properties studied were chemical composition, binder content, particle size distribution, powder morphology, interface chemistry, thermogravimetry, phase composition, and specific surface area. Among the characterization data, the binder-related properties of the powder correlated most strongly with the thermal rupture test data. Specifically, higher binder contents were associated with poor thermal rupture test performance.

Keywords binder content, plasma spray, powder characterization, powder performance correlation, thermal rupture test, yttria-stabilized zirconia powder, zirconia-based thermal barrier coatings

1. Introduction

PLASMA sprayed coatings of metallic and ceramic materials are used for a variety of gas turbine engine applications. These include abradable seals and coatings for wear resistance, dimensional restoration, and thermal protection. Variations in the quality and performance of zirconia-based thermal barrier coatings occur due to differences in the feedstock powder properties and equipment parameters (Ref 1-4). Improvements in plasma spray equipment and optimization of appropriate plasma spray parameters have been addressed to minimize variations in the coating properties. In spite of these improvements, variations in coating quality still persist (Ref 5). Some reasons may be a lack of control of appropriate powder properties and lack of information on correlations between the powder properties and powder behavior during the plasma spray coating process. A collaborative research project was conducted jointly between Pratt and Whitney (P&W) and the Ceramics Division at the National Institute of Standards and Technology (NIST) to investigate interrelationships between the powder properties and the performance in the thermal rupture test (TRT) of coatings made from those powders. To accomplish this objective, one of the primary tasks was to develop selected procedures for characterization of these powders.

Current powder specifications typically address bulk chemistry and particle size distribution related parameters. However, these parameters do not completely describe powder properties (Ref 6) and their response during processing. In addition to the powder properties usually measured, potential characteristics influencing the powder and subsequent performance include amount of binder and its distribution, morphology of particles, packing density, powder chemistry (bulk and surface), mass loss after heat treatment, and phase composition.

The primary objectives of the research reported here are: (a) to determine the differences in the physical and surface chemical properties of two types of powders, one of which consistently produced acceptable coatings (a "good" powder) and one which did not (a "bad" powder); and (b) to identify correlations between the powder properties and performance of thermal barrier coatings in the TRT. A distinguishing feature of the bad powder is that the coating produced from it contained many defects and a low TRT value. The high TRT values reported here show that a high number of samples survived this test. The powder and coating manufacturers may use these data to establish powder specifications that can be used to increase coating property repeatability and quality.

2. Powder Characterization Procedure and Results

2.1 *Materials*

(Certain trade names and company products are mentioned in the text or identified in illustrations to specify the experimental procedure and equipment used. In no case does such identification imply recommendation or endorsement by the National Institute of Standards and Technology, nor does it imply that the products are necessarily the best available for the purpose.)

Eight samples of zirconia powders of different batches, as received from the same supplier, nominally containing 20 mass% Y_2O_3 were purchased by P&W and supplied to NIST. The supplier informed P&W that these powders were processed by spray drying with a proprietary binder. All eight samples designated as A to H met the primary specifications for chemical com-

P. Pei, S.G. Malghan, and **S.J. Dapkunas,** Ceramics Division, MSEL, National Institute of Standards and Technology, Rm. 256/Bldg. 223, Gaithersburg, MD 20899, USA, and **P.H. Zajchowski,** Pratt and Whitney, United Technologies, 400 Main Street, M/S 165-34, East Hartford, CT 06108, USA.

position and particle size distribution (PSD). Table 1 lists the composition of these powders with respect to the binder, zirconia, and yttria contents. Table also lists results of the TRT (described in more detail in section 2.9) conducted on coatings made by plasma spray deposition of these powders. Based on the TRT results (percentage passing the TRT) as listed in Table 1, samples A, B, C, G, and H were identified as "good" (their percentage passing was high), and samples D and E were "bad" (their percentage passing was low). The remaining sample F was identified as acceptable.

The mass fraction of binder content ranged from 0.85 to 1.5%. Bad samples, D and E, contain the largest amount of binder (1.5%) while the remaining samples contain <1.0% binder. Yttria in these samples ranged from 19.5 to 21.5 mass%. The bad samples, D and E, have the lowest amount of yttria (19.5%), and a good sample, G, has the highest amount of yttria (21.5%).

Table 1 Specifications of powder samples and thermal rupture data

Sample	Selected chemical composition(a), mass fraction, %		Binder, mass fraction, %	Pass of the thermal rupture, test(b), %
	ZrO_2	Y_2O_3		
A	78.5	19.90	0.85	72
B	78.22	20.19	0.95	100
C	77.68	20.31	1.17	76
D	78.8	19.52	1.50	34
E	78.8	19.52	1.50	24
F	78.15	20.29	0.99	50
G	76.70	21.49	1.04	98
H	78.42	19.92	0.90	95

(a) The mass percentage data provided by powder manufacturers does not equal 100% because ZrO_2 is calculated as a difference of 100 minus total of impurities and Y_2O_3 composition. (b) This represents the percentage of the total number of thermal rupture tests of the same powder lot, that did not have cracks over a given size or did not have cracks over a certain number when all panels were subjected to the same number of thermal cycles.

Table 2 Comparison of cumulative mass fractions in the powders, mass percentage finer than stated size

Particle size, μm	Powder samples, mass fraction, %							
	A	B	C	D	E	F	G	H
-176	100	100	100	100	100	100	100	100
-125	94.5	96.7	95.8	97.8	97.8	95.3	96.6	95.0
-88	85.8	79.5	76.8	85.2	85.2	79.1	82.2	78.5
-62	68.7	56.8	53.2	60.3	60.3	57.1	60.3	55.2
-44	49.1	34.7	29.8	32.6	32.6	34.8	38.1	31.1
-31	36 8	17.4	13.6	15.5	15.5	18.8	19.8	15.5
-22	23.0	6.4	5.0	6.2	6.2	7.6	6.1	5.1
-16	14.0	1.4	1.7	1.4	1.4	2.0	2.8	3.2
-11	9.1	0	0.5	0.0	0	0.4	0.5	1.7
-7.8	6.5	0	0	0	0	0	0	0
-5.5	6.5	0	0	0	0	0	0	0
-3.9	3.7	0	0	0	0	0	0	0
-2.8	1.5	0	0	0	0	0	0	0

Particle size data are per Pratt and Whitney procedure (dry method) using Leeds and Northrup Microtrac

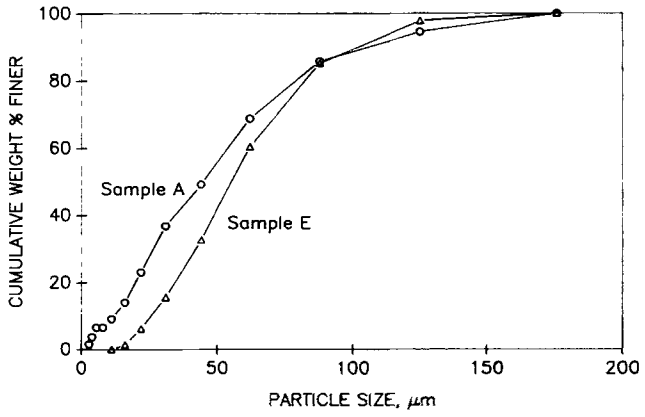

Fig. 1 Cumulative particle size distribution of samples A and E by Microtrac instrument

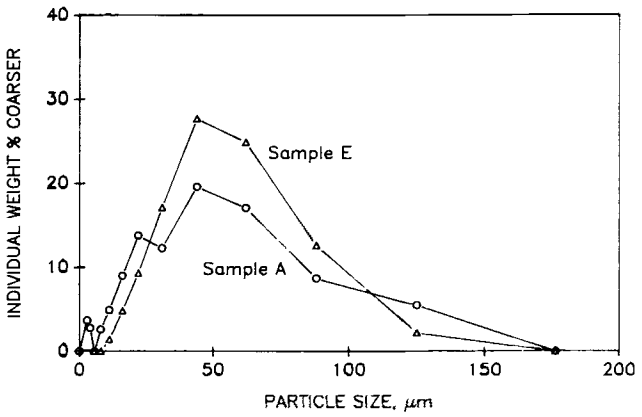

Fig. 2 Individual particle size distribution of samples A and E by Microtrac instrument

2.2 *Particle Size Distribution (PSD)*

The PSD of all eight powders was determined by the powder supplier and P&W using Microtrac instruments (Leeds and Northrup, St. Petersburg, FL). These instruments are based on the use of light diffraction data for PSD measurement. The PSD measurements were made in the dry mode because the binder used in the powder processing was known to be water soluble.

Table 2 lists the PSD measurement data. Sample A (a good powder) contained a significant amount of material, 9.1% (mass fraction), with a particle size less than 11 μm and exhibited the highest amount in the 16 to 22 μm range. Samples A, D, and E have the lowest amount of coarse fraction (88 to 125 μm). Figure 1 illustrates the presence of a high mass fraction of fine powder in sample A in comparison to that in sample E. Figure 2 illustrates a measured nonuniform PSD of sample A. The data are expressed as individual mass percentage coarser than a given size (for example, the individual mass of powder A coarser than 88 μm is the mass greater than 88 μm and less than 125 μm) to highlight the difference in PSD of good and bad powders. These data show some generalized trends in PSD of powders and highlight differences between the good and bad powders. However, not all differences are common to all good and bad powders.

2.3 *Optical Microscopy*

Optical micrographs at 125× were taken on a Leitz METALLUX 3 (E. Leitz, Rockleigh, NJ) microscope after heating the powder samples to 520 °C and in some cases to 1000 °C. Photographs were taken of a representative sample of each powder (0.02 g) sprinkled sparingly onto double-sided sticky tape that was attached to a microscope slide.

Figures 3 and 4 show the micrographs of good and bad powders of samples A and E, respectively: (a) in as-received form (Fig. 3a and 4a), (b) after 520 °C heat treatment (Fig. 3b and 4b), and (c) after 1000 °C heat treatment (Fig. 3c and 4c). No significant differences between the powders are apparent from these micrographs.

These micrographs illustrate that each sample has a wide PSD ranging from about 1 μm to 120 μm. Large clusters of particles, often consisting of smaller agglomerates, were found in each sample. In addition, a small number of doughnut-shaped agglomerates were detected in samples F and G (Fig. 5 and 6). The presence of such agglomerates indicates that hard agglomerates may have formed during spray drying (Ref 7). The agglomerates are considered to be hard when the constituting particles are held together by forces stronger than the van der Waals attractive interaction. Primarily, these doughnut-shaped agglomerates are formed due to nonuniform heat transfer from the agglomerate during spray drying of slurry droplets. In addition, in this particular situation, heterocoagulation due to hydroxylation of particle surfaces and steric forces imparted by the binders could be involved in forming strongly held agglomerates. After heat treatment at 520 °C for 20 h, the doughnut-shaped agglomerates were still present in the samples. The doughnut-shaped agglomerates are not desirable because they hinder constant flow rate of the powder in the plasma spray system (Ref 7).

One good sample (A) and one bad sample (E) were heated to 1000 °C and held for 1 h. The heat treated samples were microscopically examined at room temperature to compare with the samples before heat treatment (Fig. 3a and 4a). The micrographs (Fig. 3c and 4c) showed that the good sample A had more small particles after heating than the bad sample E. The presence of an increased number of small particles after 1000 °C heating indicates that the agglomerates have undergone shrinkage due to binder burnout. The dark-shaded spots that appear in both good and bad samples no longer exist after this heating process. The dark-shaded spots were binder-held agglomerates, which were not visible after heating.

2.4 *Tap Density*

A dual autotap (Quantachrome Corp., Syosset, NY) apparatus was used to determine the tap density of powders according to the modified ASTM procedure (ASTM B527-85). The tap density after each tapping interval (100, 300, 500, 1000, 2000, and 3000 taps) was calculated. Since the tap densities did not increase after 2000 taps, the values reported in Table 3 for all powders are steady-state values determined after 3000 taps.

Table 3 Physical and surface chemical properties of spray-dried powders

Sample	Tap density 3000 taps(a), g/cm^3	pH_{iep}(b)	Mass loss, 20 h heating, %			Net mass loss at 685 °C(c), %	Net mass loss at 520 °C(d), %	Mass binder, reported by the manufacturer, %
			100 °C	520 °C	685 °C			
A	2.06	5.4	0.25 ± 0.03	1.31 ± 0.04	1.56	1.31	1.06	0.85
B	2.06	5.4	0.09 ± 0.01	0.88 ± 0.01	0.85	0.76	0.70	0.95
C	2.21	5.3	0.20 ± 0.05	1.19 ± 0.15	1.45	1.25	0.99	1.17
D	2.00	4.5	0.20 ± 0.05	1.39 ± 0.15	1.68	1.48	1 19	1.5
E	1.98	4.9	0.34 ± 0.01	1.71 ± 0.01	1.86	1 52	1.37	1.5
F	2.05	5.4	0.20 ± 0	1.12 ± 0.05	1.34	1.14	0.92	0.99
G	2.07	5.3	0.14 ± 0	1.08 ± 0.14	1.42	1.28	0.94	1.04
H	2.07	5 3	0.17 ± 0	1 04 ± 0.04	1.22	1.05	0 87	0.90

Note: Uncertainties are estimated with duplicate analyses as one standard deviation. (a) Tap density uncertainty is ±0.02 g/cm^3. (b) pH_{iep} uncertainty is ±0 1. (c) Net mass loss percentage at 685 °C is mass loss percentage at 685 °C minus mass loss percentage at 100 °C. (d) Net mass loss percentage at 520 °C is mass loss percentage at 520 °C minus mass loss percentage at 100 °C.

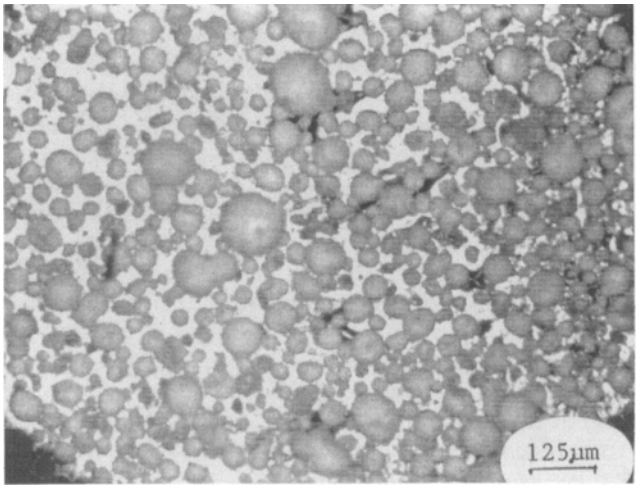

(a)

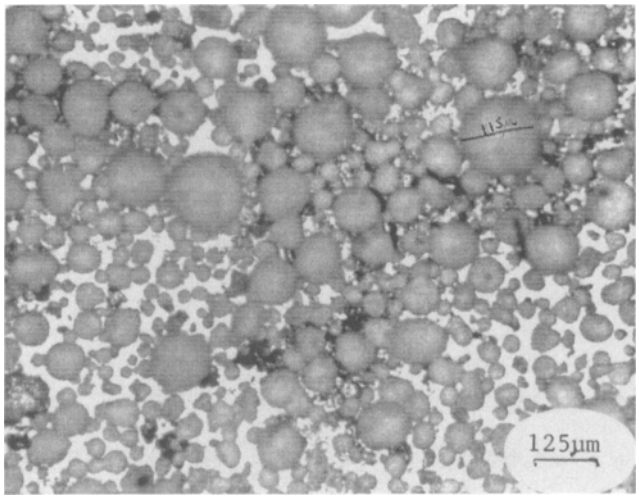

(b)

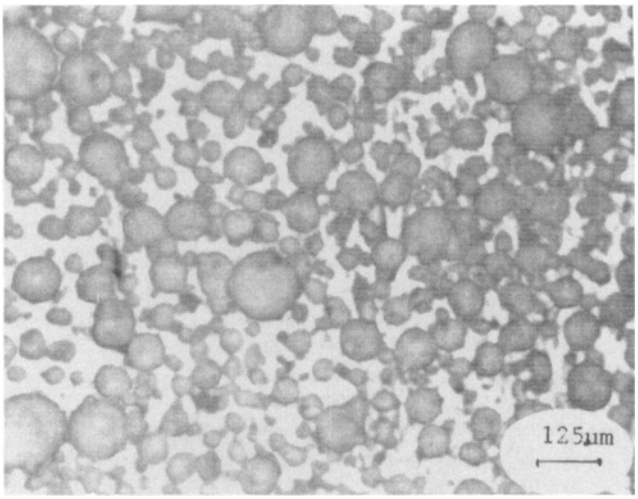

(c)

Fig. 3 Optical microscopy, micrograph of sample A at 116× (a) before heating, (b) after heating at 520 °C (20 h), and (c) after heating at 1000 °C (20 h)

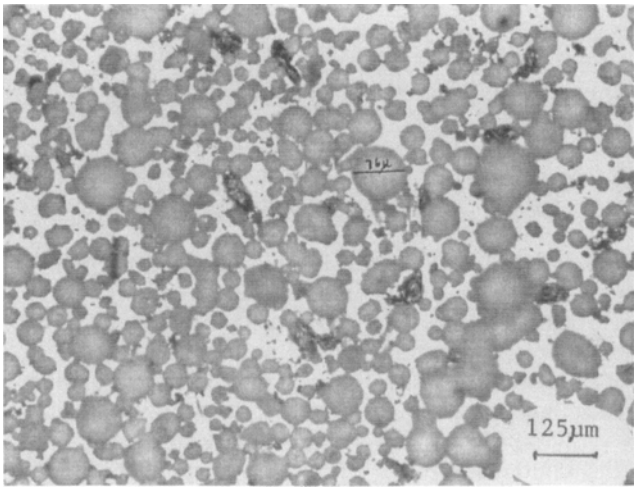

(a)

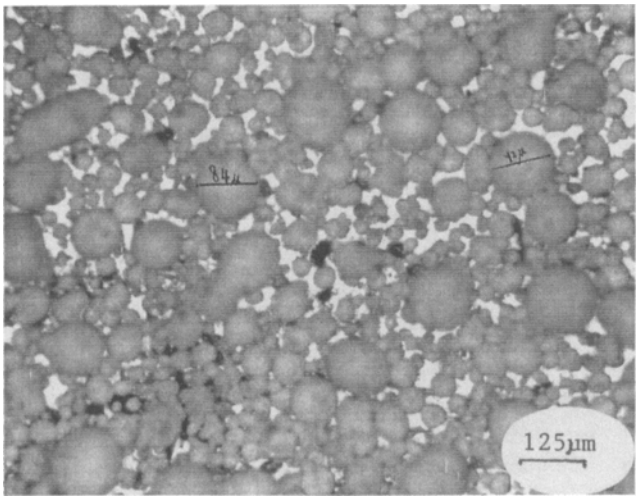

(b)

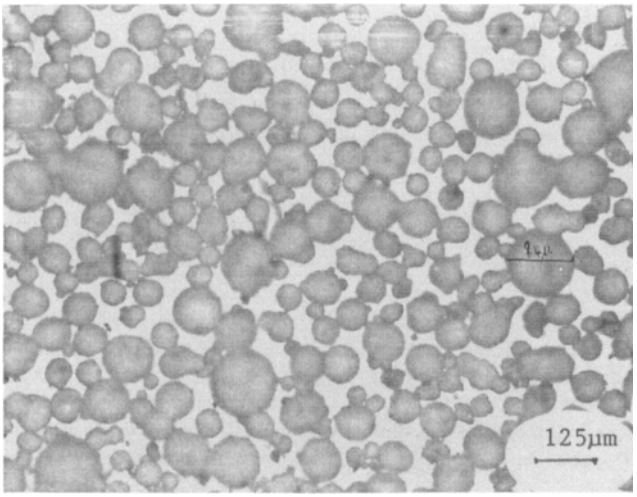

(c)

Fig. 4 Optical microscopy, micrograph of sample E at 116× (a) before heating, (b) after heating at 520 °C (20 h), and (c) after heating at 1000 °C (20 h)

Tap density is a measure of how closely the particles can arrange in a packed volume. Especially for nonspherical particles, the differences in the tap densities also indicate the flow behavior of powders in packed beds. Since some amount of degradation of agglomerates can occur during the tap density measurements, this method provides only a measure of qualitative differences among the powders. The tap density profile of a good sample A and a bad sample E are compared in Fig. 7. The tap density of sample A reaches a higher value than that of sample E. The difference in the tap densities of the good versus bad samples is primarily related to the presence of a greater proportion of larger agglomerates and the ability of fine particles to fill interstitial voids in the good samples.

2.5 *Electrokinetic Sonic Amplitude (ESA) Measurements*

The ESA measurements were obtained using the Matec ESA 8000 system (Matec Applied Sciences, Hopkinton, MA). For ESA measurements, a 5% volume fraction of slurry was prepared in 200 cm^3 deionized water and sonicated at 90 W with a sonic horn for 3 periods of 3 min sonication and 3 min cooling. The final slurry was cooled to room temperature in an ice bath. The ESA measurements were obtained by potentiometric titration as a function of pH. Detailed procedures for the sample preparation, ESA measurements, and pH_{iep} determination are reported in Ref 8. The pH of the suspension at which the net surface charge on the particles is zero is termed as the isoelectric point, pH_{iep}. The ESA measurements provide information on the interface properties of the powder in equilibrium with a liquid. In this case, the ESA data provide information on interface chemistry existing in the slip prior to spray drying. These data are highly relevant because they determine the interface chemistry existing during the formation of agglomerates.

The pH_{iep} of these powders ranged from 4.5 to 5.4 (Table 3). Figure 8 shows typical ESA response as a function of pH for good (A and B) and bad (D and E) samples. The pH_{iep} values of good samples were in the range of 5.3 to 5.4 pH, while those of bad samples ranged from 4.5 to 4.9. The differences in the pH_{iep} as well as the ranges are the result of differences in the amount and distribution of the binder and binder chemistry. The apparent general association of high pH_{iep} of powder, which performed well in the TRT and contained lower levels of binder, was confirmed by correlation analysis. Figure 9 illustrates the high correlation coefficient (CC) of 0.89 between the pH_{iep} and binder content of powders. (CC values were based on a first order of regression and calculated with a Sigmaplot software package.)

2.6 *Thermogravimetric Analysis (TGA)*

The binder content of these powders varied from 0.85 to 1.5% (Table 1). The bad samples with low TRT values had a higher binder content (1.5%), and the good samples had a lower binder content (0.85 to 1.17%). Additional TGA tests were conducted at different temperatures to characterize this binder content more accurately.

Weight loss of as-received powders was monitored as a function of heating time at a fixed heating rate (10 °C/min) from 25 to 650 °C using a Netzsch simultaneous thermal analyzer (Model STA 409, Netzsch-Geratebau, Germany). For each TGA test, the sample mass was in the range of 150 to 200 mg of the received powder. The typical response of mass loss with temperature increase is shown in Fig. 10 for A (good) and E (bad) samples

The mass loss response of powders is divided into three regions characterized by approximately three temperature ranges: up to 200 °C, 240 to 370 °C, and above 370 °C. These three temperature ranges are approximately the same for all eight powders, which indicates that the same binders were used in the spray drying process. The measure of distinct regions of mass loss is probably due to the fact that often the binders may contain two or more constituents that vaporize at different temperatures (Ref 9). One feature of these powders is that the weight loss continues beyond 680 °C, possibly due to loss of molecular water or dehydroxylation of powder.

Based on these results, follow-up experiments were conducted on the mass loss of larger samples (28 to 35 g of the as-

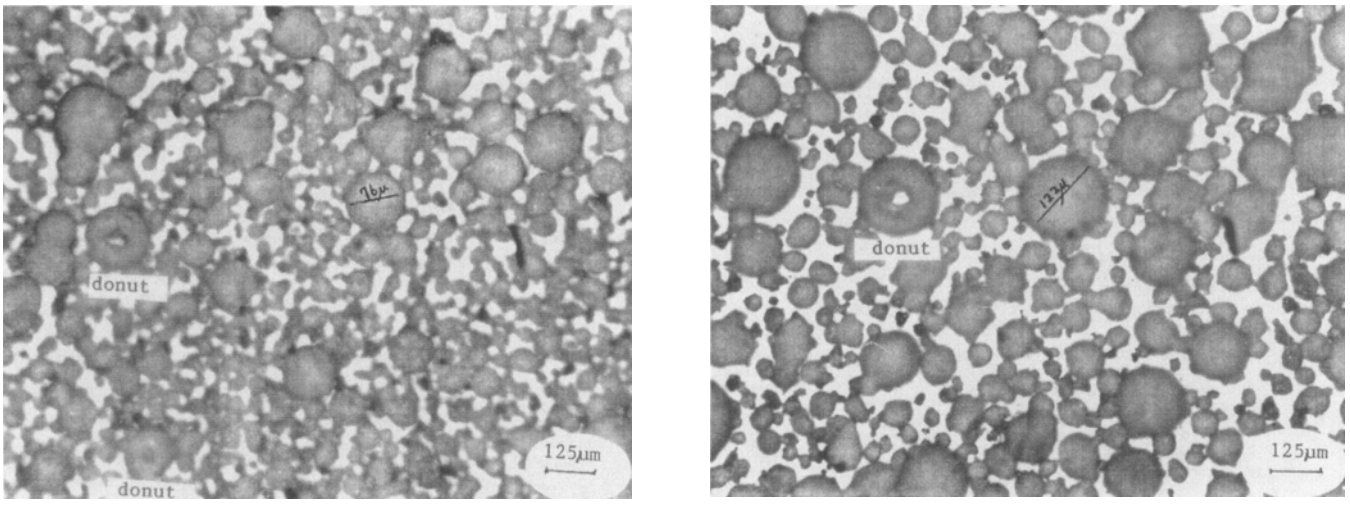

Fig. 5 Optical microscopy, micrograph of sample F at 92× (a) before heating (b) after heating at 520 °C (20 h)

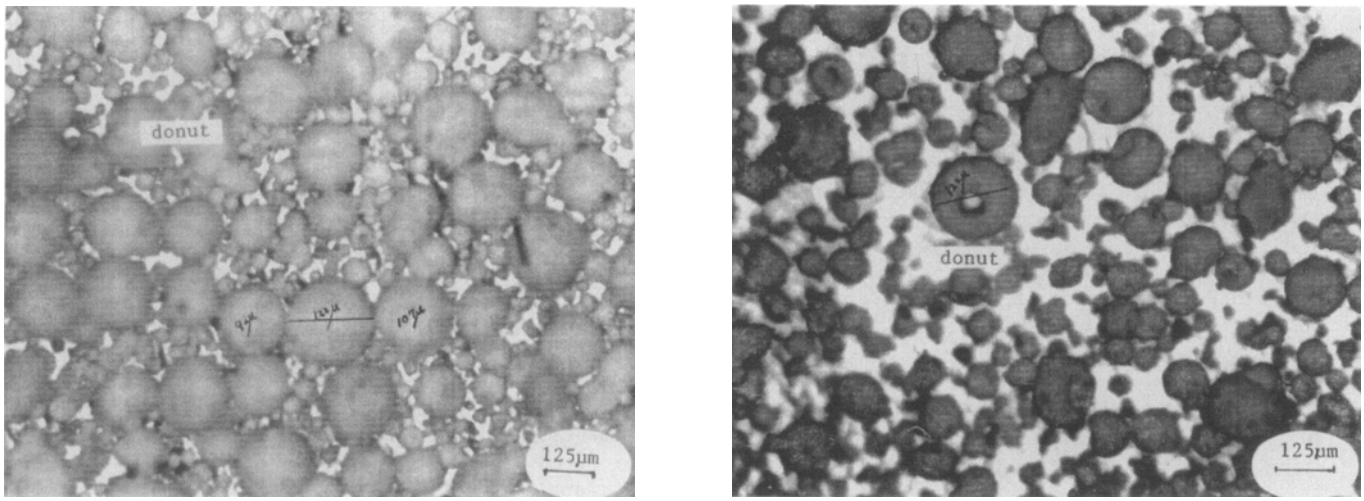

(a) (b)

Fig. 6 Optical microscopy, micrograph of sample G at 92× (a) before heating and (b) after heating at 520 °C (20 h)

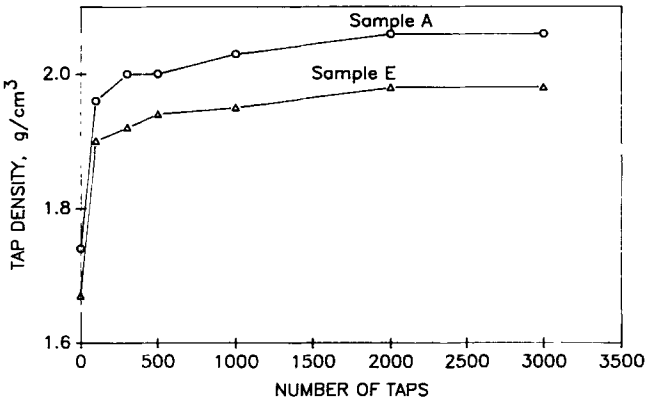

Fig. 7 Comparison of tap density of powders A and E

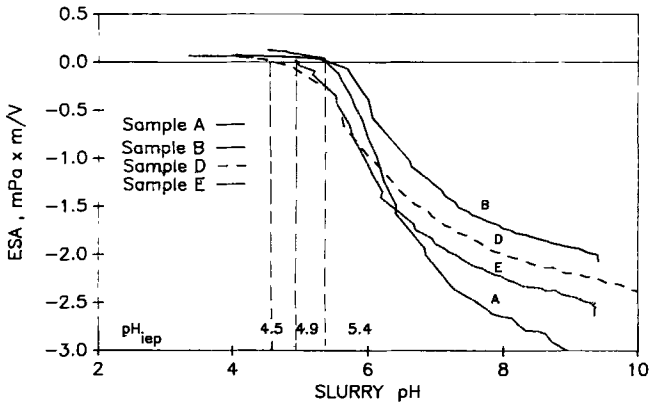

Fig. 8 Comparison of ESA plots of good (A and B) and bad (D and E) samples

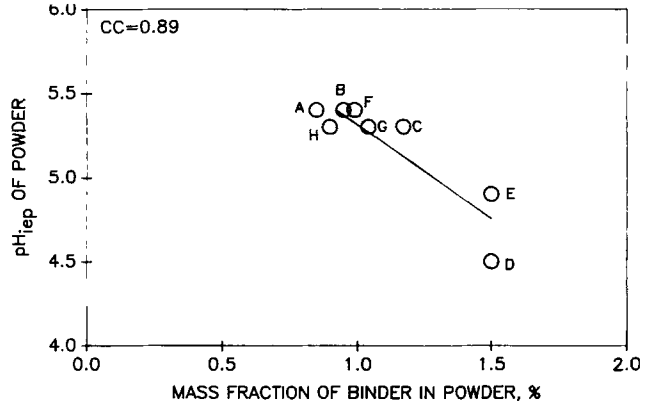

Fig. 9 Correlation between pH_{iep} and mass percentage of binder

received sample) due to prolonged heat treatment (20 h) at 100 and 520 °C. In addition, the mass loss data at 685 °C were determined by TGA. The mass loss data in the three regions are shown in Table 3. The repeatability of the mass loss data was not as good for samples C and D as evident from the larger standard deviation of the mass loss after each heat treatment. The hygroscopic nature of the binder was suspected to be the cause.

The mass loss after 520 °C heat treatment for 20 h should have a 1 to 1 correlation (CC = 1) with the amount of binder reported by the powder manufacturer if all physically held water has been lost by treatment at 100 °C and no molecular water is lost at 520 °C. The correlation plot in Fig. 11 shows a CC of 0.79 between the binder content and net mass loss at 520 °C, indicating that the entire mass of binder was not lost. The net mass loss of powders due to binder burnout was calculated by subtracting the mass of moisture lost at 100 °C from the weight loss at 685 and 520 °C (Table 3). From the data in Table 3, the following observations were made. Bad powders (samples D and E) have a net mass loss at 685 °C, which is very similar to the amount of binder reported by the manufacturer. In general, good powders have a higher net mass loss at 685 °C (except sample B) than the amount of binder reported.

2.7 *X-Ray Diffraction (XRD)*

The XRD spectra were taken on Philips diffractometers (Philips Electronics North America, New York, NY, USA) at

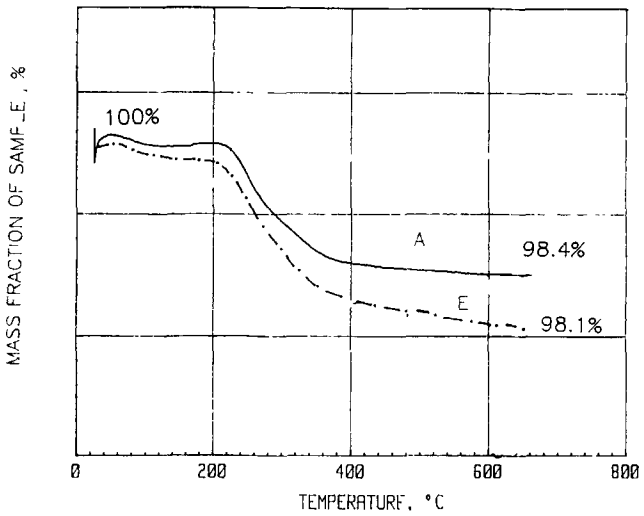

Fig. 10 Comparison of TGA plots of samples A and E

NIST. No spectral differences between the two samples were observed; hence, no further analysis was carried out.

2.8 *Specific Surface Area (SSA)*

The SSA was determined by the Brunauer-Emmett-Teller (BET) technique using a Quantasorb instrument (Quantachrome, Syosset, NY). The SSA measurements on good sample A and bad sample E showed no major differences. For example, sample A had a SSA of 3.0 m^2/g, and sample E had 2.7 m^2/g with an uncertainty of ± 0.2 m^2/g.

2.9 *Thermal Rupture Test (TRT)*

The TRT subjects a "standard" test panel to a repeatable front surface and back-side temperature transient that simulates jet engine conditions and results in a repeatable stress cycle on the panel. This thermal condition produces a stress that can cause a crack in the ceramic coating. In practice, three test panels that are 5.08 by 6.99 by 0.254 cm (2 by 2.75 by 0.1 in.) are plasma sprayed in the same fixture ring as the parts. These test panels are ground to a standard configuration and tested in a thermal rupture rig where they undergo a rapid temperature cycle on the top side of the panel while being air cooled on the bottom side.

After testing, the panels are visually and microscopically examined, and the lengths of the cracks are measured. The ring of parts is accepted or rejected based upon the average crack length for the three panels. A high pass percentage TRT value means that coatings produced from those powders passed this test with lower average crack lengths.

3. Analysis of the Characterization Results

3.1 *Binder Content*

A plot of TRT values versus mass percentage binder with a CC of 0.78 is shown in Fig. 12. Higher mass percentage binder yielded lower acceptance TRT values. The parameter "mass percentage binder" represents binder related factors, such as binder distribution, binder composition, and binder interaction with particles. Figure 13 shows the correlation between pH_{iep} and TRT with a CC of 0.71. The pH_{iep} is a measure of both binder distribution in the powder and interaction of binder and particles with water. Figures 14 (a) to (c) show the correlations between the net mass loss after heat treatment at 100, 520, and 685 °C and TRT values. The highest CC of 0.85 was obtained for the mass loss after 520 °C heat treatment. This net mass loss is a measure of binder content.

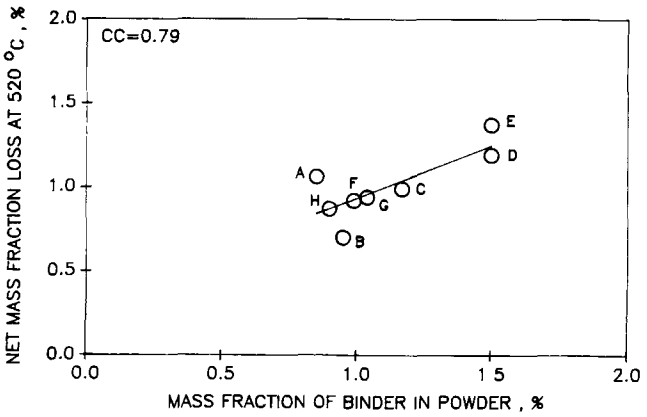

Fig. 11 Correlation between mass percentage of binder and net mass percentage loss after treatment at 520 °C

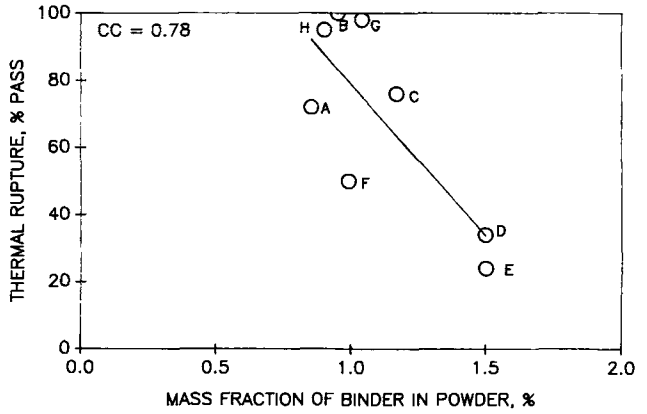

Fig. 12 Correlation between thermal rupture (pass percentage) data and mass percentage of binder

It was suspected that when the binder is not evenly distributed among the particles, it might form aggregates that vaporize at higher temperatures during the plasma coating process or the TRT. Vaporization of these binder aggregates might form voids or pits in the plasma coatings and increase the chance of failing the TRT.

3.2 *PSD*

In general, the binder composition and binder content have a strong relationship with the PSD of spray-dried powders (Ref 10). The strength, morphology, and size distribution of powder agglomerates is greatly influenced by the dispersion of particles and uniformity of the binder distribution in the slurry and spray

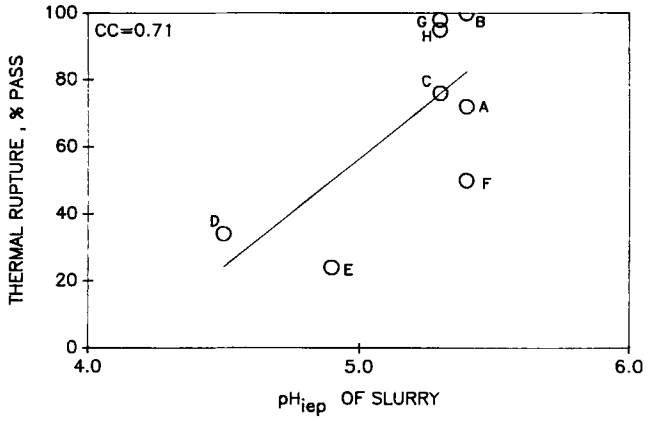

Fig. 13 Correlation between thermal rupture (pass percentage) data and pH_{iep} of slurry

dryer parameters. Variation in these parameters can lead to change in the characteristics of the resulting powders.

Optical microscopic studies show the presence of both large (over 100 μm) and small (about 20 μm) particles, a reflection of the variabilities in the spray drying process. Black spots, observed in the as-received powders, presumably of binder aggregates, were absent in the powders that were heated to 1000 °C. Volatilization of the binder, only after heating to 1000 °C, indicates that some of the binder may be strongly held in the spray-dried agglomerates.

The correlation between the TRT values versus PSD by Microtrac dry analysis was not as good as that of TRT versus binder specific measurements. Figure 15 shows the correlation plots of individual mass at >88 μm and between 44 to 62 μm versus the TRT values. The CC values were 0.53 and 0.66, respectively. The low values do not mean that no correlations exist. The lack of high CC values could be due to insensitivity of the PSD measurement procedure to identify relevant parameters in the PSD. In general, mass of large particles increases as the TRT percentage increases with the exception of powder A. On the contrary, the individual mass in the smaller particle size range 44 to 62 μm increases as the TRT percentage decreases (see Fig. 15a and b). This observation agrees with that published by the National Aeronautics and Space Administration (NASA) study (Ref 11). The NASA study concluded that the coarse powders yielded a coating of considerable amount of porosity and a slight degree of microcracking, which released thermal stresses. This resulted in higher TRT values. Finer size powders would produce coatings of dense structure and lower TRT values.

3.3 *Tap Density*

Figure 16 shows the correlation between tap densities at 3000 taps of all eight samples and pass percentage of the TRT. A trend toward higher TRT acceptance values of the powders at higher tap densities was shown, but the CC was small (0.53). A powder with a larger quantity of coarse particles yielded a lower tap density as fine particles filled the voids between the large particles and produced a higher tap density.

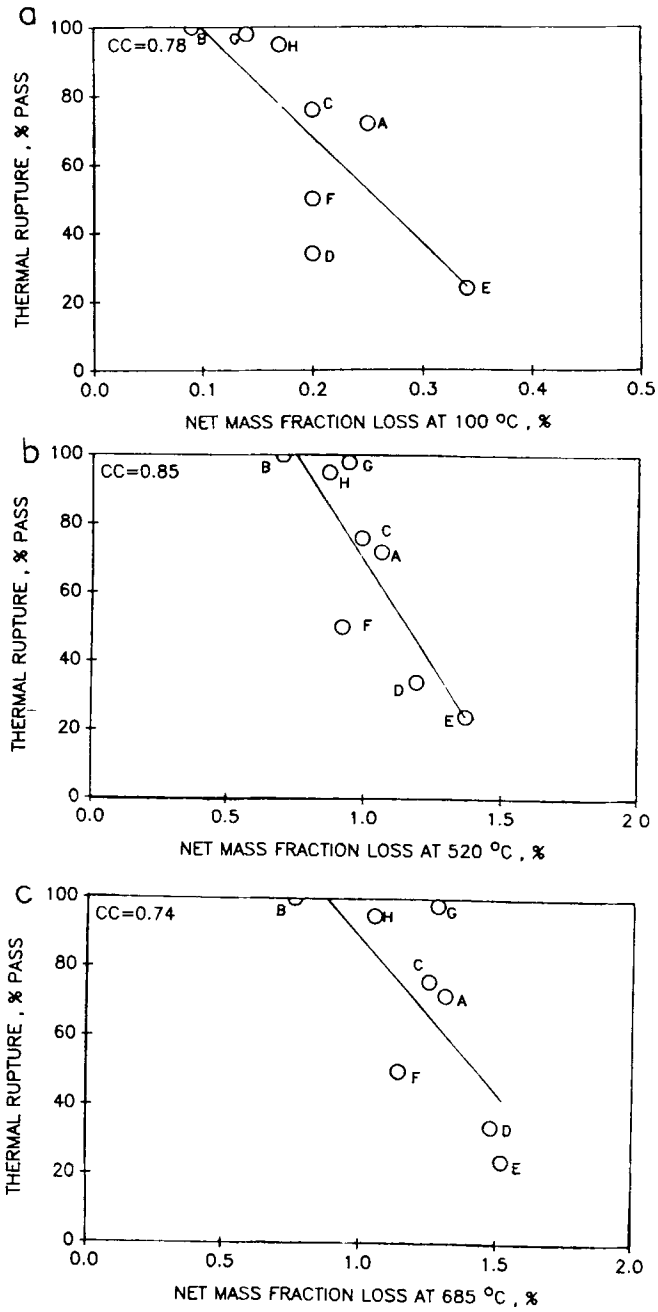

Fig. 14 Correlation between thermal rupture (pass percentage) data and net percentage mass loss at (a) 100 °C, (b) 520 °C, and (c) 685 °C

4. Conclusions

Eight spray-dried zirconia powders containing 20 mass% yttria were characterized for their physical and chemical properties. Correlations were made between the binder parameters, such as binder composition, binder content, binder distribution, binder aggregation, powder weight loss, agglomerate morphology, and agglomerate size distribution, and the TRT performance of coatings deposited from the same powder. Among these data, the binder content, pH_{iep}, net weight loss after 520 °C heat treatment, and PSD showed reasonably good correlations

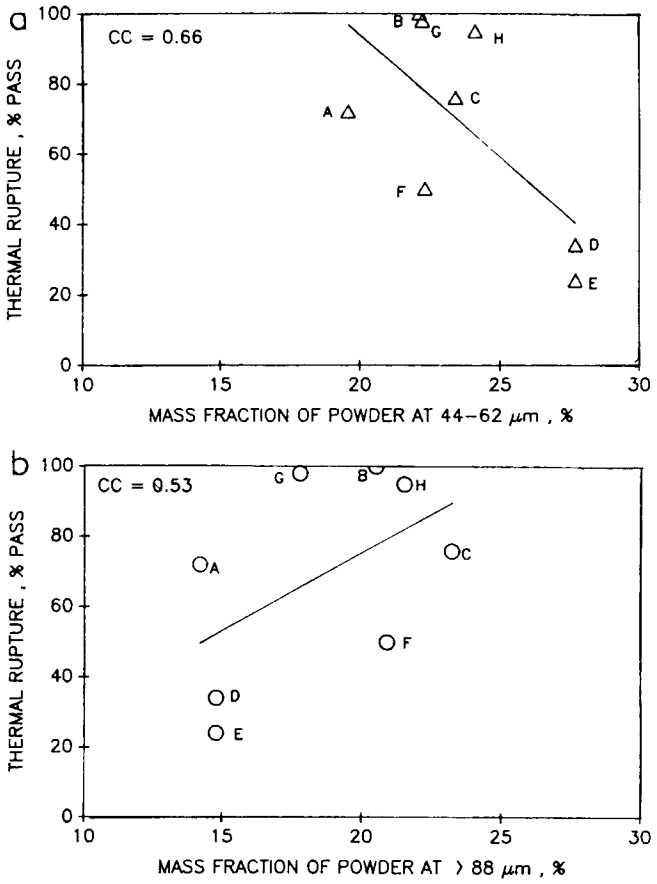

Fig. 15 Correlation between thermal rupture (pass percentage) data and mass percentage of powders at (a) 44 to 62 μm and (b) >88 μm

with the TRT data. The binder content of the powder appears to be related to TRT data more than the PSD. Since both pH_{iep} and net weight loss after 520 °C are related to the binder content, a good correlation evidently exists between the TRT data versus pH_{iep} and the mass percentage loss after heat treatment.

Based on the results and analysis reported here, powder specifications that characterize binder parameters should be addressed. Some of the specific characterization methods that should be included are thermal analysis for binder composition and concentration, electrokinetics by ESA for binder interface chemistry, uniformity of binder coating on particles and binder chemistry, and optical image analysis for agglomerate morphology, agglomerate size distribution, and binder aggregation.

Acknowledgments

This research is based on a collaborative project between the National Institute of Standards and Technology and Pratt and Whitney during 1990. Work was performed under contract F33657-86-C-0011 as part of a project sponsored by Aeronautical Systems Center (AFMC) Wright-Patterson AFB, Ohio. The

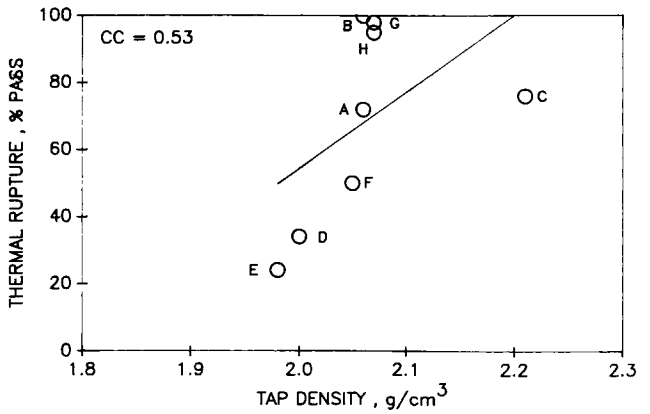

Fig. 16 Correlation between thermal rupture (pass percentage) data and tap density of powders

authors are thankful to Dr. J. Wallace for TGA analysis, Mr. D. Minor for specific surface area data, and Dr. J. Cline for XRD data. Also thanked are G. Gruver, G. Foster, R. Roark, and C. Bevan of Pratt and Whitney for their assistance and cooperation during this study.

References

1. I.A. Fisher, Variables Influencing the Characteristics of Plasma-Sprayed Coating, *Int. Mater. Rev.*, Vol 17, 1972, p 117-129
2. R.A. Miller, Current Status of Thermal Barrier Coatings—An Overview, *Surf. Coat. Technol.*, Vol 30, 1987, p 1-11
3. M. Vardelle, A. Vardelle, and P. Fauchais, Spray Parameters and Particle Behavior Relationships During Plasma Spraying, *J. Therm. Spray Technol.*, Vol 2, 1993, p 79-92
4. T.E. Mantkowski, D.V. Rigney, M.J. Froning, and N Jayaraman, Characterization of ZrO_2-Y_2O_3 Thermal Spray Powder Systems, *Proceedings of the Material Research Society-Europe Conference on Coatings for Heat Engines*, Material Research Society-Europe, Nov 1985, p 41-56
5. A.R. Nicoll and H. Eschnauer, Retesting Thermal-Spray Powders, *Surf. Coat. Technol.*, Vol 30, 1987, p 95-106
6. E.J. Kubel, Jr., Powders Dictate Thermal Spray Coating Properties, *Adv. Mater. Process.*, December 1990, p 24-32
7. S.J. Lukasiewicz, Spray-Drying Ceramic Powders, *J. Am. Ceram. Soc.*, Vol 72 (No. 4), 1989, p 617-624
8. V.A. Hackley and S.G. Malghan, Investigation of Parameters and Secondary Components Affecting the Electroacoustic Analysis of Silicon Nitride Powders, *Electroacoustics for Characterization of Particulates and Suspensions*, S.G. Malghan, Ed., NIST SP856, National Institute of Standards Technology, 1993, p 161-179
9. Y.N. Sun, M.D. Sacks, and J.W. Williams, Pyrolysis Behavior of Acrylic Polymers and Acrylic Polymer/Ceramic Mixtures in Ceramic Transaction, *Ceramic Powder Science, II A*, Messing, E.R. Fuller, Jr., and H. Hausner, Ed., 1, 1988, p 538-548
10. S.G. Malghan, R.S. Premachandran, and P.T. Pei, Mechanistic Understanding of Silicon Nitride Dispersion Using Cationic and Anionic Polyelectrolytes, *Powder Technology*, Vol 79, 1994, p 43-52
11. K.D. Sheffler, R.A. Graziani, and G.C. Sinko, "JT9D Thermal Barrier Coated Vanes," Rep. NASA-CR-167964, NASA Center, April 1982